

Angle-resolved x-ray absorption near edge structure study of vertically aligned single-walled carbon nanotubes

Zhongrui Li,^{a)} Liang Zhang, and Daniel E. Resasco
*School of Chemical, Biological and Materials Engineering, University of Oklahoma,
 Norman, Oklahoma 73019*

Bongjin Simon Mun
Material Science Division, Lawrence Berkeley National Laboratory, Berkeley, California 94720

Félix G. Requejo
*Departamento de Física and INIFTA-IFLP (CONICET), Universidad Nacional de La Plata, 1900 La Plata,
 Argentina*

(Received 11 October 2006; accepted 23 January 2007; published online 8 March 2007)

Vertically aligned single-walled carbon nanotube (SWNT) forest was studied by using angular-dependent C *K*-edge x-ray absorption near edge structure (XANES) with linearly polarized x-ray beam. The XANES analysis found a crust of entangled nanotubes on top of the forest formed at the first stage of the forest growth, which shapes the morphology of the entire forest and constricts the nanotubes to grow to the same length. It indicates that this type of SWNT forest has a different growth mechanism from the multiwalled carbon nanotube forest. © 2007 American Institute of Physics. [DOI: 10.1063/1.2709506]

Aligned carbon nanotubes have potential applications in field emission as well as in high-strength materials. Probing orientation of single-walled carbon nanotube (SWNT) systems is of paramount importance in these fields. By using linearly polarized x-ray beam, angular-dependent x-ray absorption near edge structure (XANES) spectroscopy provides such a capability to investigate the order of SWNTs.¹ Since XANES detects transitions in carbon from the highly isotropic *1s* core level, any polarization dependence will reflect the anisotropy of the final states. The dipole transition matrix elements thus have an angular dependence on the angle made by, for instance, the π^* orbital with respect to the electric field vector of the incident polarized x rays. Thus, changes in the intensity of the resonances upon rotating the sample in the plane of incidence of the beam provide evidence for bond orientation. Recently, the angle-resolved XANES gains increasing attention in the carbon nanotube study.^{2,3} With this technique Chiou *et al.* found enhanced π^* and σ^* intensities at the tips of multiwalled carbon nanotube (MWNT) arrays.⁴ In this work, we use angular-dependent carbon *1s* XANES measurements to study the anisotropy of vertically aligned SWNT forest grown on the silicon wafer. Angle-resolved XANES demonstrated very useful for the order measurement and the aligned growth mechanism study of carbon nanotubes.

The angle-resolved C *K*-edge XANES spectra were taken in total electron yield (TEY) mode under UHV (low 10^{-10} torr) at beamline 9.3.2 of Advanced Light Source in Lawrence Berkeley National Laboratory. The XANES data were collected at various angles ranging from $\theta=10^\circ$ (“glancing”) to $\theta=80^\circ$ (“normal”), where θ denotes the angle between the sample normal and the direction of the electric vector of the x-ray beam. In order to correct the transmission function of the monochromator all measured spectra were normalized to photon flux, obtained from the current yield of

a clean Au grid placed before samples. The monochromator energy scale was calibrated using carbon *K*-edge π^* transition of graphite, located at 285.35 eV. The vertically aligned SWNTs were prepared on a *p*-type Si wafer by catalytic chemical vapor deposition method, as described elsewhere.⁵ Using scanning electron microscope (SEM) and transmission electron microscope, the well vertically aligned SWNTs were observed to be about 37 μm long and approximately 2 nm in diameter [Figs. 1(a) and 1(b)].

The TEY XANES spectra measured at different incident angles were shown in Fig. 1(c). The C *K*-edge XANES spectra of the SWNT forest are quite similar to those of graphite.^{6,7} The sharp excitons at 285.4 and 291.5 eV are attributed to the dipolar transition of core level *1s* electron into the C–C π^* and C–C σ^* states in the conduction band, respectively. Two other σ^* transitions from 292 to 298 eV and broad ($\sigma+\pi$) transitions from 301 to 309 eV are also observed. Two small peaks in 287–290 eV can be assigned to the oxygenated surface functionalities, perhaps associated with the defects of the nanotubes. According to Kuznetsova *et al.* these peaks might correspond to π^* C=O and σ^* C–O (or σ^* C–H) resonances.⁸

The angular dependence of the π^* and σ^* excitations can be understood by studying the electronic structure. Simultaneous calculations of x-ray absorption spectra and the density of states (DOSs) were performed with *ab initio* self-consistent real space multiple-scattering code FEFF 8.4.⁹ The FEFF simulation is compared with the spectrum collected at “magic angle” of 54.7° , where π^* and σ^* transitions are independent of the molecular orientation (Fig. 2). The overall features of the *p*-like DOS are reproduced, although the peak position and the intensity are different. The energy differences are due to the difference in relaxation energy for the various final states, which the one-electron DOS does not take into account. It is difficult to reproduce the π^* bond with FEFF due to the muffin-tin scattering potential approximations. Nevertheless, the angular dependence of XANES for

^{a)} Author to whom correspondence should be addressed; electronic mail: lizhongrui@gmail.com

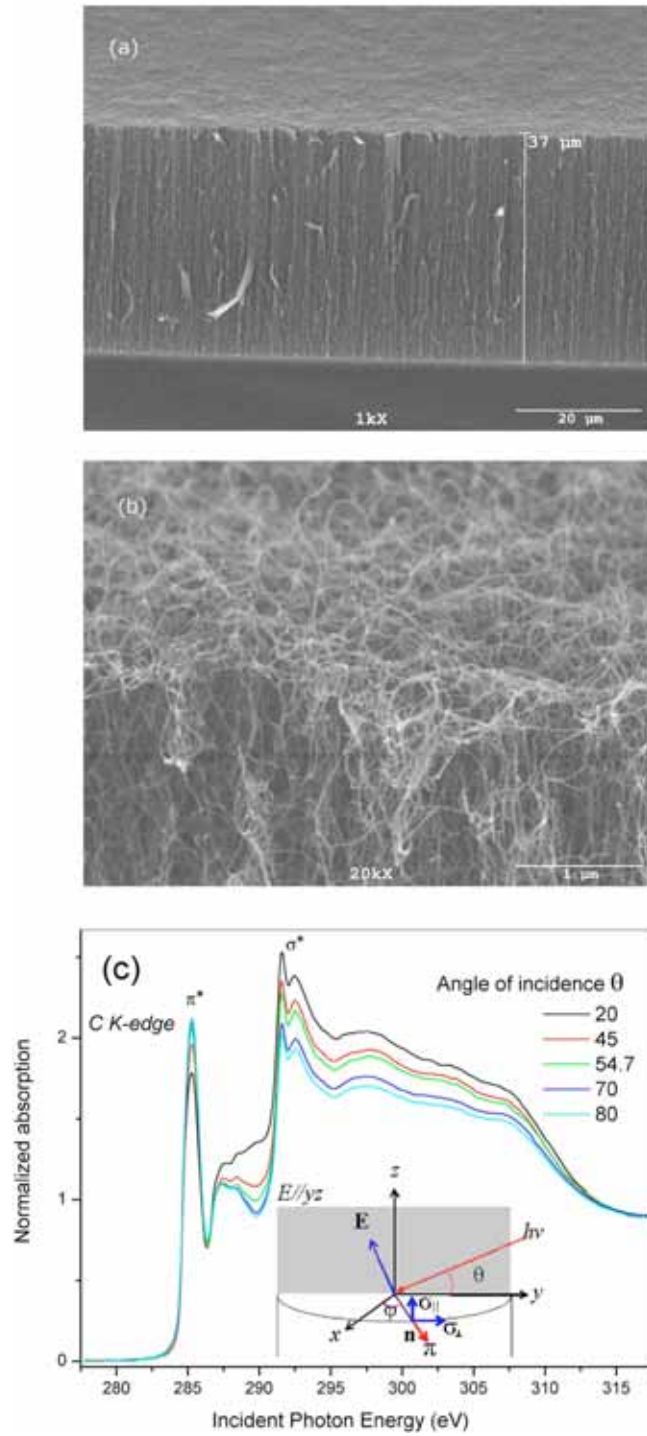


FIG. 1. (Color online) (a) Side and (b) 60° top views of typical SWNT forest produced on silicon wafer observed by SEM. (c) Angle-resolved TEY XANES spectra of SWNT forest grown on silicon wafer. The inset shows the incident geometry of π^* vector orbitals and σ^* planes for a vertical SWNT tube (axis along z) on Si wafer with respect to the incident beam and the electric field vector E which remains perpendicular to the incident x-ray beam.

vertically aligned SWNT forest predicted by FEFF does follow the trend as observed in our case.

To quantitatively understand the above results, we proceed to evaluate the angular dependencies that would be expected for the three possible orientations of nanotubes (as in Ref. 10). According to Fermi's golden rule, the transition probability can be expressed as

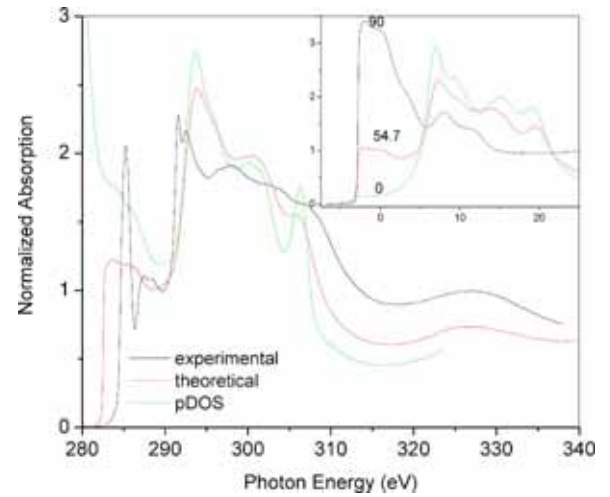


FIG. 2. (Color online) *Ab initio* simulation of XANES of vertical SWNT forest at magic angle (incidence angle 54.7°) with FEFF 8.4 code using the same geometry as shown in the inset of Fig. 1(c). The inset displays the simulated angular-dependent XANES spectra of vertically aligned SWNT forest.

$$I \propto |\langle f | \mathbf{E} \cdot \mathbf{r} | i \rangle|^2 = |\mathbf{E} \cdot \langle f | \mathbf{r} | i \rangle|^2 = A \cos^2 \delta,$$

where f and i are the final and initial wave functions, respectively. \mathbf{E} is the electric field vector, \mathbf{r} is the position vector, and δ is the angle between the \mathbf{E} vector and position vector \mathbf{r} . With a simple calculation by accounting all contributions on the entire tube circumference, we found that the π^* and σ^* intensities for the vertical SWNT forest show sine-squared and cosine-squared dependences, respectively (tube axis in z direction, Table I). It is easy to understand, for instance, that the σ^* resonance can be viewed as a combination of two perpendicular components, one is parallel to tube axis direction (σ_{\parallel}^*) and another along circumferential direction [σ_{\perp}^* also perpendicular to the tube axis, see the inset of Fig. 1(c)]. The local contribution to the σ^* intensity is proportional to the sum of the squared scalar products of the two components and electric polarization vector. Electric vector has a larger projection along the tube axis (σ_{\parallel}^*) at glancing incidence, thus the σ^* resonance is at its maximum. At normal incidence, electric vector is normal to σ_{\parallel}^* , only part of σ_{\perp}^* orbitals contributes the intensity, so σ^* has the lowest intensity. The σ_{\parallel}^* intensity is proportional to $2 \cos^2 \theta$ while the σ_{\perp}^* has a $\sin^2 \theta$ dependence. Therefore, in total the σ^* intensity decreases when the x-ray incidence angle changes from grazing to normal, i.e., cosine-squared dependence.

In order to quantitatively analyze the angular dependencies of these different contributions in the XANES spectra, the TEY XANES spectra were fitted to a series of pseudo-Voigt functions, an arctangent step corresponding to

TABLE I. The angular dependence of the π^* and σ^* intensities of carbon nanotube under the following geometries. The incident beam and its electric vector are in the yz plane, c and θ denote the tube axis and the angle between the z axis and the electric vector of the x-ray beam [see the inset of Fig. 1(c)], respectively ($\sigma^* = \sigma_{\parallel}^* + \sigma_{\perp}^*$).

Tube axis	π^*	σ^*	σ_{\parallel}^*	σ_{\perp}^*
x ($\mathbf{E} \perp c$)	1	1	0	1
y ($\mathbf{E} \parallel c$)	$\cos^2 \theta$	$1 + \sin^2 \theta$	$2 \sin^2 \theta$	$\cos^2 \theta$
z (v tube)	$\sin^2 \theta$	$1 + \cos^2 \theta$	$2 \cos^2 \theta$	$\sin^2 \theta$

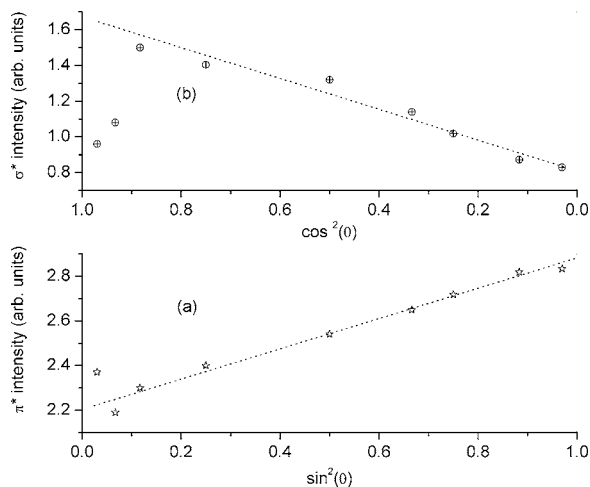


FIG. 3. Integrated intensities of the π^* and σ^* resonances vs sine-squared and cosine-squared functions. Errors in the integrated areas are about $\pm 5\%$.

the excitation edge of carbon and a background by following the method proposed by Outka *et al.*¹¹ For all spectra, a fit was considered acceptable only if it can reproduce the data and the second derivative of the data. As shown in Fig. 3, the intensities of the π^* and σ^* excitons generally show sine-squared and cosine-squared dependences, respectively. However, deviations have been observed in both π^* and σ^* intensities at glancing angle. Concomitant with these deviations, the orientation parameter [OP = $(I_{\perp} - I_{\parallel}) / (I_{\perp} + I_{\parallel})$] from the π^* intensities at normal and parallel incidences was calculated to be 0.145, smaller than that seen in highly oriented pyrolytic graphite (0.902).¹⁰ It is consistent with the presence of some randomly distributed tubes which cover the top of the SWNT forest (tube axis in xy plane) and add residual intensity to the resonances most noticeable at glancing angles. In fact, the only very top layer (crust) of the forest has the nanotubes with parallel orientation [Fig. 1(b)]. Immediately below this crust, the orientation is preferentially vertical. The presence of a disordered structure on the top of the forest was also observed by others.^{12,13} It indicates that, at the beginning of a SWNT forest growth, SWNTs grow at different rates with random orientation over the surface and weave a crust of entangled SWNTs, then a concerted growth of vertically aligned SWNT is constrained by the uniform top crust.

Additionally, the two oxygen-associated resonances between 287 and 290 eV increase with decreasing x-ray incidence angle. The remarkable increase of the C–O feature at small incidence angle can be also attributed to the increased surface sensitivity of TEY XANES at a glancing angle. The larger π^* C=O and σ^* C–O resonances at glancing angle indicate that the C–O and C=O bonds are likely polarized perpendicular to the crust of the forest, which is also consistent with the crust structure oriented parallel to the surface.

Obviously, our observation for the vertically aligned SWNT forest is different from that of MWNT forest.⁴ For the case of the MWNT array, an increase of the x-ray absorption intensity with the increase of incidence angle was observed not only for the unoccupied π^* states but also for the σ^* state because of the enhanced DOSs of both unoccupied π^* and σ^* bands at the tip. However, our vertically aligned SWNT forest does not show enhanced density of states at tips by reason of the crust on the top of the SWNT forest. It also suggests that this type of SWNT structure has a different growth mechanism as compared with the MWNT array, which has no crust structure in its growth.

In summary, the angle-resolved XANES of a SWNT forest in TEY shows that the C–C π^* resonance intensity decreases from normal to glancing incidence, while the C–C σ^* exhibits an opposite trend, which can be used to evaluate the order of SWNTs. A crust of entangled SWNT on top of the forest was found parallel to the surface as a result of different growth rates of individual tubes in the first step of the forest growth, which is responsible for the unique forestlike morphology exhibited by this type of SWNT structures. It is different from the growth of MWNT forest.

Financial support from DOE Basic Energy Sciences (Grant No. DE-FG03-02ER15345) and NSF (Grant No. CTS-0308619) is gratefully acknowledged. One of the authors (F.G.R.) acknowledges to projects PICT03 06-17492 (ANPCyT, Argentina) and 14116-120 (Fundación Antorchas, Argentina).

¹J. Stöhr, *NEXAFS Spectroscopy* (Springer-Verlag, Berlin, 1992).

²J. Schiessling, L. Kjeldgaard, F. Rohmund, L. K. L. Falk, E. E. B. Campbell, J. Nordgren, and P. A. Bruhwiler, *J. Phys.: Condens. Matter* **15**, 6563 (2003).

³Y. H. Tang, T. K. Sham, Y. F. Hu, C. S. Lee, and S. T. Lee, *Chem. Phys. Lett.* **366**, 636 (2002).

⁴J. W. Chiou, C. L. Yueh, J. C. Jan, H. M. Tsai, W. F. Pong, I.-H. Hong, R. Klauser, M.-H. Tsai, Y. K. Chang, Y. Y. Chen, C. T. Wu, K. H. Chen, S. L. Wei, C. Y. Wen, L. C. Chen, and T. J. Chuang, *Appl. Phys. Lett.* **81**, 4189 (2002).

⁵L. Zhang, Y. Tan, and D. Resasco, *Chem. Phys. Lett.* **422**, 198 (2006).

⁶P. Skytt, P. Glans, D. C. Mancini, J.-H. Guo, N. Wassdahl, J. Nordgren, and Y. Ma, *Phys. Rev. B* **50**, 10457 (1994).

⁷S. Banerjee, T. Hemraj-Benny, M. Balasubramanian, D. A. Fischer, J. A. Misewich, and S. S. Wong, *ChemPhysChem* **5**, 1416 (2004).

⁸A. Kuznetsova, I. Popova, J. T. Yates, Jr., M. J. Bronikowski, C. B. Huffman, J. Liu, R. E. Smalley, H. H. Hwu, and J. G. Chen, *J. Am. Chem. Soc.* **123**, 10699 (2001).

⁹A. L. Ankudinov, C. E. Bouldin, J. J. Rehr, J. Sims, and H. Hung, *Phys. Rev. B* **65**, 104107 (2002).

¹⁰S. Banerjee, T. Hemraj-Benny, S. Sambasivan, D. A. Fischer, J. A. Misewich, and S. S. Wong, *J. Phys. Chem. B* **109**, 8489 (2005).

¹¹D. Outka, J. Stöhr, J. P. Rabe, and J. D. Swalen, *J. Chem. Phys.* **88**, 4076 (1988).

¹²S. Maruyama, E. Einarsson, Y. Murakami, and T. Edamura, *Chem. Phys. Lett.* **403**, 320 (2005).

¹³Y. Q. Xu, E. Flor, M. J. Kim, B. Hamadani, H. Schmidt, R. E. Smalley, and R. H. Hauge, *J. Am. Chem. Soc.* **128**, 6560 (2006).

Applied Physics Letters is copyrighted by the American Institute of Physics (AIP). Redistribution of journal material is subject to the AIP online journal license and/or AIP copyright. For more information, see <http://ojps.aip.org/aplo/aplcr.jsp>